buildings

MDPI

Article

Finite Element Modeling and Artificial Neural Network Analyses on the Flexural Capacity of Concrete T-Beams Reinforced with Prestressed Carbon Fiber Reinforced Polymer Strands and Non-Prestressed Steel Rebars

Hai-Tao Wang [1], Xian-Jie Liu [1], Jie Bai [2,*], Yan Yang [2,*], Guo-Wen Xu [2] and Min-Sheng Chen [1]

[1] College of Civil and Transportation Engineering, Hohai University, Nanjing 210098, China; cewht@hhu.edu.cn (H.-T.W.); 231304020012@hhu.edu.cn (X.-J.L.); 201304020001@hhu.edu.cn (M.-S.C.)
[2] Shanghai Engineering Research Center of CFRP Application Technology in Civil Engineering, China Construction Eighth Engineering Division Co., Ltd., Shanghai 200122, China; xuguow@cscec.com
* Correspondence: baijie@cscec.com (J.B.); yangyan0615@cscec.com (Y.Y.)

Abstract: The use of carbon fiber reinforced polymer (CFRP) strands as prestressed reinforcement in prestressed concrete (PC) structures offers an effective solution to the corrosion issues associated with prestressed steel strands. In this study, the flexural behavior of PC beams reinforced with prestressed CFRP strands and non-prestressed steel rebars was investigated using finite element modeling (FEM) and artificial neural network (ANN) methods. First, three-dimensional nonlinear FE models were developed. The FE results indicated that the predicted failure mode, load-deflection curve, and ultimate load agreed well with the previous test results. Variations in prestress level, concrete strength, and steel reinforcement ratio shifted the failure mode from concrete crushing to CFRP strand fracture. While the ultimate load generally increased with a higher prestressed level, an excessively high prestress level reduced the ultimate load due to premature fracture of CFRP strands. An increase in concrete strength and steel reinforcement ratio also contributed to a rise in the ultimate load. Subsequently, the verified FE models were utilized to create a database for training the back propagation ANN (BP-ANN) model. The ultimate moments of the experimental specimens were predicted using the trained model. The results showed the correlation coefficients for both the training and test datasets were approximately 0.99, and the maximum error between the predicted and test ultimate moments was around 8%, demonstrating that the BP-ANN method is an effective tool for accurately predicting the ultimate capacity of this type of PC beam.

Keywords: prestressed concrete beams; CFRP strands; flexural behavior; finite element modeling; artificial neural network

check for updates

Citation: Wang, H.-T.; Liu, X.-J.; Bai, J.; Yang, Y.; Xu, G.-W.; Chen, M.-S. Finite Element Modeling and Artificial Neural Network Analyses on the Flexural Capacity of Concrete T-Beams Reinforced with Prestressed Carbon Fiber Reinforced Polymer Strands and Non-Prestressed Steel Rebars. *Buildings* **2024**, *14*, 3592. https://doi.org/10.3390/buildings14113592

Academic Editor: Francisco López-Almansa

Received: 21 October 2024
Revised: 5 November 2024
Accepted: 11 November 2024
Published: 12 November 2024

Copyright: © 2024 by the authors. Licensee MDPI, Basel, Switzerland. This article is an open access article distributed under the terms and conditions of the Creative Commons Attribution (CC BY) license (https://creativecommons.org/licenses/by/4.0/).

1. Introduction

Applying prestress to concrete structures to form prestressed concrete (PC) structures can significantly improve the mechanical behavior of ordinary reinforced concrete (RC) structures by enhancing crack resistance and normal serviceability [1]. As a result, PC structures are widely used in civil infrastructure, such as long-span prestressed concrete bridges. Typically, prestressed steel rebars and steel strands are employed as prestressed reinforcement in PC structures. However, due to the corrosion-prone nature of steel, the corrosion problem of prestressed steel reinforcement poses serious safety risks to PC structures in harsh environments [2,3]. The section loss of prestressed steel rebars and stands caused by corrosion may lead to the sudden collapse of prestressed RC structures. For example, the recent collapse of the Carola Bridge in Germany, a prestressed concrete bridge, is suspected to have been caused by corrosion of the internal steel reinforcements due to the penetration of large amounts of chlorides [4]. On the other hand, once corrosion occurs, replacing these internally prestressed reinforcements is challenging, making strengthening

measures essential, which can be both time-consuming and costly. Therefore, to ensure the service safety and longevity of PC structures, it is crucial to enhance the corrosion resistance of the prestressed reinforcement itself.

Over the past three decades, fiber reinforced polymer (FRP) has been widely used to strengthen existing structures due to its high strength and excellent corrosion resistance [5–14]. The types of FRP commonly used in civil engineering include carbon-FRP (CFRP), basalt-FRP (BFRP), and glass-FRP (GFRP), depending on the type of fiber used [15–17]. Numerous studies have shown that prestressed FRP is significantly more effective than non-prestressed FRP in enhancing the mechanical behavior of both concrete and steel beams [18–23]. However, compared to its use in structural strengthening, the application of FRP in new concrete structures has been relatively limited, despite many relevant studies in this area [24–30]. The excellent corrosion resistance and high strength of FRP materials make them promising alternatives to prestressed steel reinforcement, offering the potential to increase the corrosion resistance of prestressed reinforcement. To explore the effectiveness of internally prestressed FRP in PC structures, some researchers have investigated PC beams reinforced with prestressed FRP bars. For example, Atutis et al. [24] studied the flexural performance of concrete beams reinforced with prestressed glass-FRP (GFRP) bars and found that increasing the prestress level in the GFRP bars significantly increased the cracking load, mitigated crack generation and propagation, and enhanced the structural stiffness compared to non-prestressed beams. Flexural tests conducted by Saafi et al. [25] revealed a notable disparity in the ultimate deflection of concrete beams reinforced with bonded and unbonded prestressed aramid-FRP (AFRP) bars, with the unbonded specimens exhibiting significantly higher deflection than their bonded counterparts. Heo et al. [26] carried out flexural tests on prestressed CFRP-reinforced concrete beams and obtained similar conclusions, further revealing a close relationship between the failure mode of the experimental beams and the sectional shape. Additionally, some theoretical and numerical studies have also been implemented in this area, given that experimental investigations often require substantial time and cost. Peng and Xue [27,28] proposed theoretical methods for calculating the ultimate capacity of concrete T-beams reinforced with prestressed FRP bars and non-prestressed FRP bars, as well as T-Beams with prestressed FRP bars and non-prestressed steel bars. Kim [30] conducted a three-dimensional nonlinear finite element (FE) analysis and iterative sectional analysis to predict the mechanical behavior of prestressed FRP-reinforced concrete beams. Lou et al. [31] employed numerical software to assess the flexural performance of post-tensioned FRP-reinforced concrete beams, finding that the number of prestressed FRP bars significantly influenced the ultimate load, ductility, neutral axis depth, and stress in the non-prestressed steel rebars. By combining experimental findings with FE simulations, Motwani et al. [32] investigated the transfer length and prestress loss characteristics of prestressed FRP bars. Bedon et al. [33] numerically analyzed post-tensioned prestressed FRP-reinforced concrete beams, focusing on initial cracks and the damage evolution process. These studies have demonstrated that prestressed FRP bars are highly effective in PC structures.

In addition to prestressed FRP bars, prestressed FRP strands have recently been utilized in PC beams [1,34]. Unlike FRP bars, one FRP strand is fabricated by twisting multiple FRP bars together [34–37]. This design allows the multiple bars within a single FRP strand to be anchored collectively in one anchor [1,36], significantly reducing the number of anchors needed. To evaluate the feasibility of carbon-FRP (CFRP) strands as prestressed reinforcement in PC structures, Wang et al. [37] conducted experimental and theoretical studies on the bond performance between CFRP strands and concrete, finding that surface-treated CFRP strands exhibited bond performance similar to that of steel strands. Static and cyclic tests on PC beams reinforced with prestressed CFRP strands have shown that CFRP strands are effective in enhancing the mechanical properties of concrete beams [1,34]. However, the previous experimental study [1] involved only a limited range of parameters, leaving the mechanical behavior of PC beams reinforced with prestressed CFRP strands incompletely explored. Therefore, further studies are necessary

to enhance the understanding of the flexural behavior of this type of PC beam. On one hand, it is crucial to investigate the effects of additional parameters on the mechanical properties, which can be implemented using FE modeling. On the other hand, developing a rapid and accurate predictive method is essential for the practical application of this type of PC beam. In recent years, the application of artificial intelligence techniques in civil engineering has garnered increasing interest. Numerous studies have aimed to predict the ultimate capacity of various structural members [38–44], such as the compressive capacity of FRP-strengthened columns and the flexural and shear capacities of FRP-strengthened beams. These studies demonstrate the efficiency and high accuracy of artificial intelligence techniques in predicting structural capacities.

Based on the above background, the FE modeling was first conducted in this study to develop a numerical prediction method for the flexural behavior of PC T-beams reinforced with prestressed CFRP strands and non-prestressed steel rebars. Using the verified FE models, the effects of prestress level, concrete strength, and steel reinforcement ratio were analyzed. Furthermore, an artificial neural network (ANN) method was employed to predict the ultimate flexural capacity. The study can deepen the understanding of the mechanical properties and provide a rapid and accurate ANN-based method for predicting the ultimate capacity, facilitating the practical applications of this type of PC beam.

2. Summary of the Experimental Study

Four-point bending tests were conducted on eight concrete T-beams to investigate the effectiveness of prestressed CFRP strands as prestressed reinforcements in PC beams, as presented in a previous study [1]. The total length of the concrete beams was 4200 mm, with a net span of 4000 mm. The T-beam flange had 400 mm in width and 75 mm in thickness, while the web had a width of 250 mm and a depth of 325 mm. The concrete beams were reinforced with either three or two hot-rolled steel rebars (the latter only in specimen BS-45R) with a diameter of 22 mm in the tension zone and four steel rebars with a diameter of 8 mm in the compression zone. Transverse stirrups with a diameter of 10 mm were spaced along the beam length, with intervals of 150 mm in the pure-bending zone and 80 mm in the two flexural-shear zones, to ensure sufficient shear resistance. The prestress was applied to concrete beams using post-tensioned CFRP strands. The detailed geometric dimensions and reinforcement arrangements of the PC beams can be found in reference [1]. All the beams were cast using commercial concrete with a strength grade of C40, which exhibited a measured cubic compressive strength of 32.6 MPa after 28 days of curing in an outdoor environment. The mechanical properties of the hot-rolled steel rebars are listed in Table 1. The CFRP strands used in the tests consisted of seven CFRP bars, each with a diameter of 5 mm, twisted together to form a nominal diameter of 15.2 mm. The cross-section area of each CFRP strand was 140 mm^2, with a guaranteed ultimate tensile strength of 2500 MPa and an elastic modulus of 170 GPa. The two anchors for the CFRP strands were secured to the PC beam using backing plates located at both ends and bolts corresponding to the anchors.

Table 1. Measured mechanical properties of the steel rebars [1].

Diameter (mm)	Yielding Strength (MPa)	Tensile Strength (MPa)	Elastic Modulus (GPa)
8	602	761	200
10	603	677	200
22	467	646	192

In addition to one ordinary RC beam as a reference specimen, seven beams were reinforced with both prestressed CFRP strands and non-prestressed steel rebars. A total of five study parameters were designed in the tests, including the prestress level, number of CFRP strands, layout of CFRP strands, presence or absence of bond layer, and steel reinforcement ratio, as shown in Table 2. In the specimen identifier, the first letter B denotes the beam, while B-0 represents the reference specimen without CFRP strands. The second letter is employed to distinguish the number of CFRP strands, and the letters S and D denote one and two CFRP strands, respectively. The following number represents the prestress level in the CFRP strands, defined as the ratio of the design's initial prestress to the ultimate tensile strength of the CFRP strand, expressed as a percentage. The last letter is used to distinguish the presence or absence of a bond layer, the layout of the CFRP strands, and the steel reinforcement ratio. Specifically, the letter U represents a specimen with an unbonded prestressed CFRP stand, the letter C denotes a specimen with a curved prestressed CFRP strand, and the letter R represents a specimen with a reduced reinforcement ratio of non-prestressed steel rebars compared to the other specimens. More design details can be found in reference [1].

Table 2. Main design parameters of test specimens and key test results [1].

Specimen	Layoaut of CFRP Strands	Prestress Level (%)	Initial Prestress (MPa)	Bonding	P_{cr} (kN)	P_y (kN)	P_u (kN)	Failure Mode
B-0	/	/	/	/	46	233	246	C
BS-30	Straight	30	750	Yes	69	280	296	C
BS-45	Straight	45	1125	Yes	80	296	318	C
BS-60	Straight	60	1500	Yes	93	317	337	C
BS-45U	Straight	45	1125	No	73	290	307	C
BS-45C	Curve	45	1125	Yes	76	294	324	C
BS-45R	Straight	45	1125	Yes	78	219	261	C
BD-30	Straight	30	750	Yes	91	323	348	C

All specimens were subjected to four-point bending tests at loading rates of 0.5 mm/min and 0.8 mm/min using a testing machine with a capacity of 1000 kN. The length of the pure bending zone was 1000 mm, and both flexural-shear zones were 1500 mm long. Two concentrated loads were applied to the beams via rigid pads placed on top of the flange, to eliminate local stress concentration at the compressive flange. The main test results, including the cracking load, yielding load, ultimate load, and failure mode, are summarized in Table 2. In the table, P_{cr}, P_y, and P_u represent the cracking load, yielding load, and ultimate load, respectively, while the letter C in the failure mode column denotes compressive concrete crushing. Experimental tests observed that as the load increased, the PC beams experienced several typical stages: cracking in the tensile concrete, yielding of the non-prestressed steel rebars, and eventually, compressive concrete crushing. Neither tensile fracture failure of the CFRP strands nor pullout failure from the anchors (i.e., anchorage failure) was observed during the tests, which demonstrated the excellent anchorage efficiency of the mechanical anchors used for the CFRP strands. The typical load-midspan deflection curves of all specimens are summarized in Figure 1. From Table 2 and Figure 1, it is evident that, compared to the reference beam B-0, the flexural behavior of all PC beams significantly improved after the addition of prestressed CFRP strands. The cracking load increased by 50.0–102.2%, the yielding load by 20.2–38.6%, and the ultimate load by 20.3–41.4%. This demonstrated the high effectiveness of prestressed CFRP strands as prestressed reinforcement in PC beams. Moreover, the prestress level was a key parameter influencing the flexural behavior. The steel reinforcement ratio also affected the flexural behavior. However, PC beams with straight and curved CFRP strands exhibited very similar flexural behavior. In addition, bonded prestressed CFRP strands provided a slight advantage over unbonded ones. The previous tests also found that, under the same prestress level, increasing the number of CFRP strands significantly enhanced the

mechanical behavior of the PC beams; however, if the total prestress force in the PC beams remained unchanged, merely increasing the number of CFRP strands had only a slight effect on the flexural behavior.

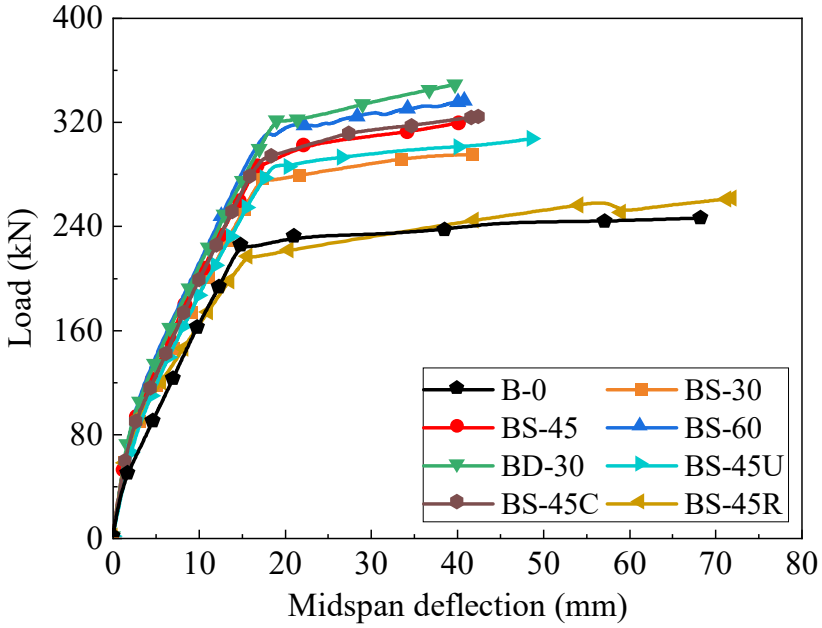


Figure 1. Load-deflection curves obtained from the experimental tests [1].

3. Finite Element Modeling

In this section, three-dimensional nonlinear FE models were established using the commercial numerical analysis software Abaqus 2020 to predict the flexural behavior of PC beams reinforced with prestressed CFRP strands and non-prestressed steel rebars. The main objectives of the FE modeling are as follows: (1) to develop an accurate flexural capacity prediction method based on numerical simulations; (2) to perform parametric analyses to evaluate the effects of the prestress level, concrete strength, and steel reinforcement ratio; and (3) to establish a database for training the ANN model.

3.1. FE Models

3.1.1. Element Types and Meshes

Due to the material and geometrical symmetry, a one-quarter model was established for each specimen. In the FE models, the concrete, CFRP stands, rigid pads, and backing plates were simulated using brick element C3D8R. The steel reinforcements were simulated by truss element T3D2. To simplify the modeling of the twisted shape of the CFRP strand, this study equated the CFRP strand to a CFRP bar with a normal diameter of 13.3 mm, ensuring that both configurations had the same cross-sectional area. While establishing the FE models, for the specimen with curved CFRP strands, the geometrical model was assembled using SolidWorks 2020 software and meshed using HyperMesh 2017 software. In contrast, the other models were developed directly using Abaqus 2020 software. Through a convergence analysis, the general mesh sizes were selected to be 30 mm. A typical FE model is shown in Figure 2.

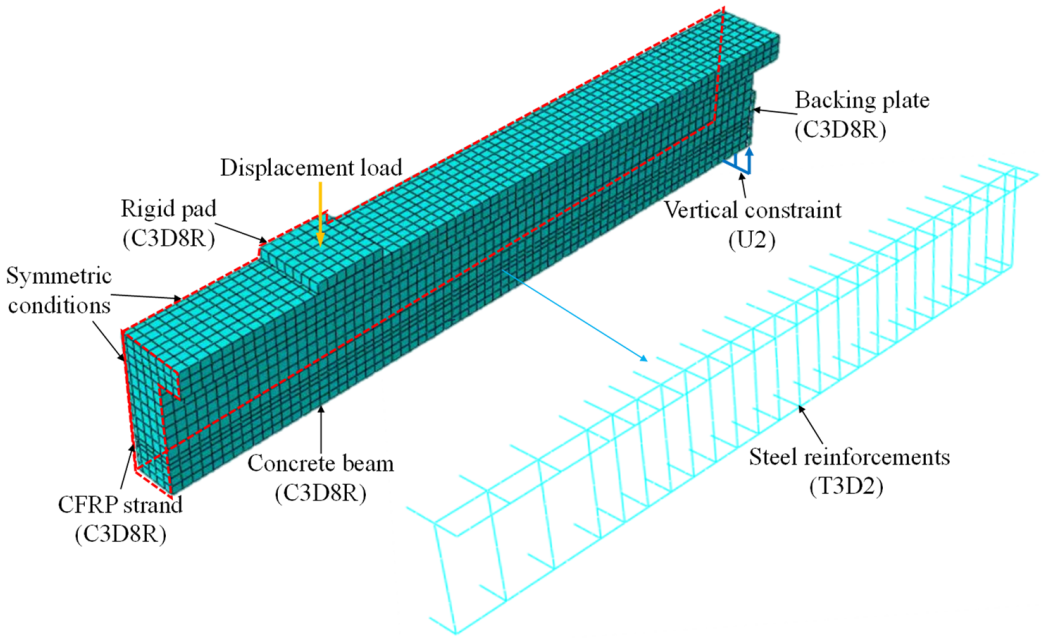


Figure 2. Typical FE model.

3.1.2. Material Properties

The Concrete Damage Plasticity (CDP) model was used to simulate the mechanical behavior of the concrete. The tensile and compressive stress–strain curves recommended in the Chinese code [45] were adopted as the constitute models for the concrete. Based on the design code and existing research [45,46], the key damage plasticity parameters are detailed in Table 3. Steel rebars were modeled as an elastic-plastic material. Based on the measured tensile stress–strain curves, a bilinear model was employed for both the 8 mm and 10 mm rebars, while a trilinear model was used for the 20 mm rebars to account for the yielding plateau. The CFRP strands were modeled as linear elastic materials with an elastic modulus of 170 GPa and Poisson's ratio of 0.3. For the backing plates and rigid pads, since no yielding occurred during the tests, a linear-elastic model with an elastic modulus of 210 GPa was applied.

Table 3. Main parameters used in concrete damage plasticity model.

Elastic Modulus (MPa)	Poisson's Ratio	Dilation Angle	Eccentricity	Compressive Strength Ratio	Stress Invariant Ratio	Viscosity Parameter
3.0×10^4	0.2	30°	0.1	1.16	0.6667	0.0005

3.1.3. Interactions and Boundary Conditions

In the FE models, the steel rebars were embedded into the concrete using the "Embedded" method. Two types of contact properties were defined for the interactions between the CFRP strands and the concrete. In the first type, the standard surface-to-surface contact was applied where the concrete surface was defined as the master surface and the strand surface as the slave surface. The contact property in the normal direction was modeled using "hard" contact. In the tangent direction, the contact property was modeled using a "penalty" function with a friction coefficient of 0.4. In the second type, the cohesive contact was defined, which accounted for the bond between the CFRP strands and the concrete. According to the reference [47], the cohesive law was applied with maximum bond stress of 5 MPa, elastic stiffness of 10 MPa/mm, and fracture energy of 5.88 N·mm. The quadratic stress criterion was employed to identify damage initiation, and the energy-based linear failure criterion was used to identify the failure. For the PC beams with bonded prestressed CFRP strands, the standard surface-to-surface contact was applied during the prestress

application stage, and the cohesive contact property was used to simulate the bond behavior between the strands and the concrete during the loading stage. For the PC beams with unbonded CFRP strands, the standard surface-to-surface contact was used in both the prestress application and loading stages, ensuring that the CFRP strands could move relative to the surrounding concrete during loading.

Both the connection between the backing plate and the PC beam, as well as the connection between the rigid pad and the PC beam, were modeled by the "Tie" constraint. Due to the excellent anchorage behavior of the anchors, they were not explicitly simulated in the models; instead, the CFRP strands were directly tied to the backing plate. The translational degree of freedom in the Y direction (U2) was constrained for all nodes along the supporting line. Additionally, the symmetrical boundary conditions were applied to the symmetrical sections of the FE models. The detailed boundary conditions are also illustrated in Figure 2.

3.1.4. Load Application

For the PC beams reinforced with prestressed CFRP strands and non-prestressed steel rebars, the concrete beams were first prepared, after which the CFRP strands were tensioned to form the post-tensioned PC beams before the application of loading. Therefore, two loading steps were applied to the FE models. In the first loading step, the gravity load of the PC beams was applied, and the initial prestress was introduced by simulating a temperature reduction in the CFRP strands. In the second step, a reference point was set and coupled to the rigid pad, and a displacement load was applied through the reference point.

3.2. Numerical Results and Model Verification

3.2.1. Comparisons of Numerical and Test Results

In the FE modeling, in addition to the test specimens, seven additional specimens were simulated to further investigate the effects of prestress level, concrete grade, and steel reinforcement ratio, as listed in Table 4. The comparisons of characteristic loads (cracking load, yielding load, and ultimate load) between the numerical and experimental results are shown in Table 4, and the numerical and experimental load-deflection curves are compared in Figure 3. In the table, Δ_u presents the ultimate deflection, which is defined as the midspan deflection at P_u, while σ_u denotes the tensile stress in the CFRP strand at P_u. The letters C and F indicate crushing failure of the compressive concrete and tensile fracture of the CFRP strands, respectively. Generally, the numerical results exhibited good agreement with the experimental results. The ratio of numerical to experimental cracking loads ranged from 0.97 to 1.09, with a relative error of within 9%. The ratio for yielding loads ranged from 0.94 to 0.98, with a relative error of within 6%. For ultimate loads, the ratio varied from 0.94 to 1.02, with a relative error of within 6%. As shown in Figure 3, the numerical load-deflection curves effectively captured the load-deflection relationship of the PC beams reinforced with prestressed CFRP strands and non-prestressed steel rebars. Additionally, the predicted failure mode for all test specimens was compressive concrete crushing, which was consistent with the test results, as compared in Figure 4 (Note: The strain contours were mirrored to display the full span of the specimens, with the gray color representing concrete compressive strain exceeding 0.0033).

Table 4. Main numerical results and comparison with test results from reference [1].

Specimen	P_{cr} (kN)			P_y (kN)			P_u (kN)			Δ_u (mm)	σ_u (MPa)	Failure Mode
	Test	FE	Ratio	Test	FE	Ratio	Test	FE	Ratio			
B-0	46	44.7	0.97	233	224.1	0.96	246	245.4	1.00	71.9	/	C
BS-30	69	73.1	1.06	280	269.2	0.96	296	297.6	1.00	44.6	1721	C
BS-45	80	86.8	1.09	296	282.9	0.96	318	307.0	0.97	40.0	1997	C
BS-60	93	97.5	1.05	317	297.1	0.94	337	317.2	0.94	35.6	2283	C
BS-45U	73	74.5	1.02	290	279.0	0.96	307	293.3	0.96	42.6	1594	C

Table 4. *Cont.*

Specimen	P_{cr} (kN)			P_y (kN)			P_u (kN)			Δ_u (mm)	σ_u (MPa)	Failure Mode
	Test	FE	Ratio	Test	FE	Ratio	Test	FE	Ratio			
BS-45C	76	79.1	1.04	294	285.2	0.97	324	316.8	0.98	43.3	2074	C
BS-45R	78	79.6	1.02	219	215.2	0.98	261	266.4	1.02	55.4	2441	C
BD-30	91	97.2	1.07	323	310.5	0.96	348	339.3	0.98	38.6	1483	C
BS-0	/	49.5	/	/	237.3	/	/	291.3	/	61.7	1357	C
BS-70	/	104.2	/	/	306.9	/	/	322.0	/	34.1	2462	C
BS-80	/	117.2	/	/	316.3	/	/	324.6	/	24.5	2500	F
BS-90	/	120.6	/	/	/	/	/	273.9	/	13.2	2500	F
BS-45R#	/	82.6	/	/	190.3	/	/	246.5	/	56.7	2500	F
BS-60-C30	/	92.2	/	/	293.7	/	/	308.5	/	33.6	2183	C
BS-60-C50	/	110.0	/	/	301.1	/	/	340.2	/	42.2	2500	F

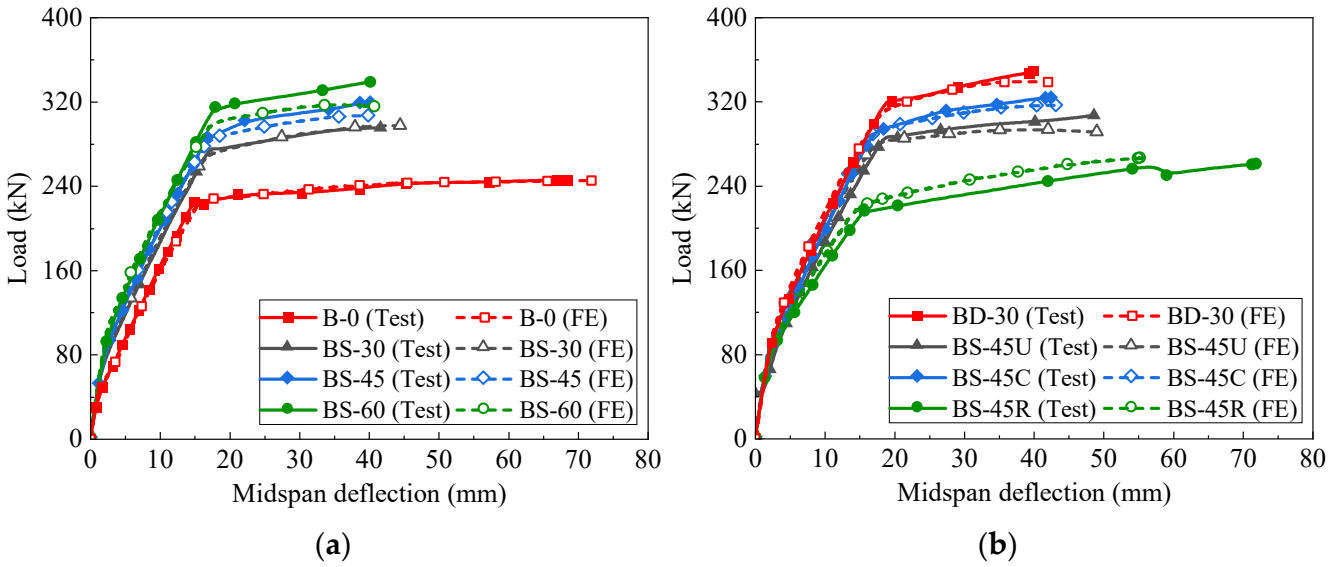


Figure 3. Comparison of the numerical and experimental load-deflection curves from reference [1]: (**a**) reference specimen and specimens with different prestress levels; (**b**) other specimens.

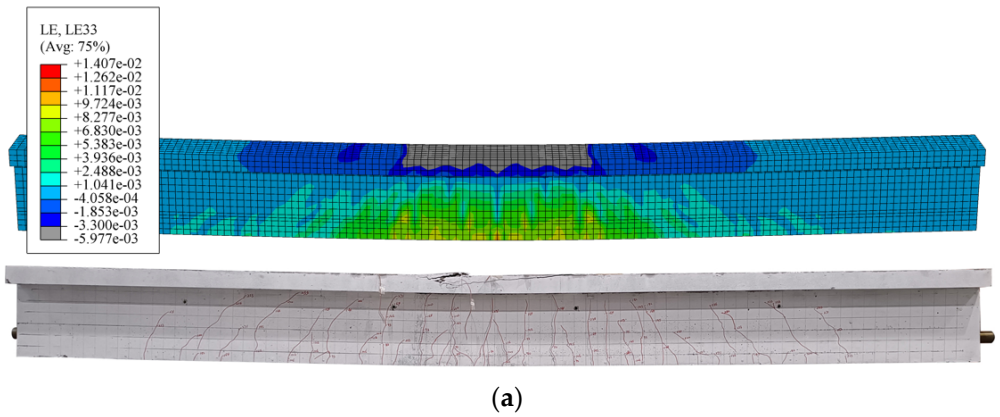
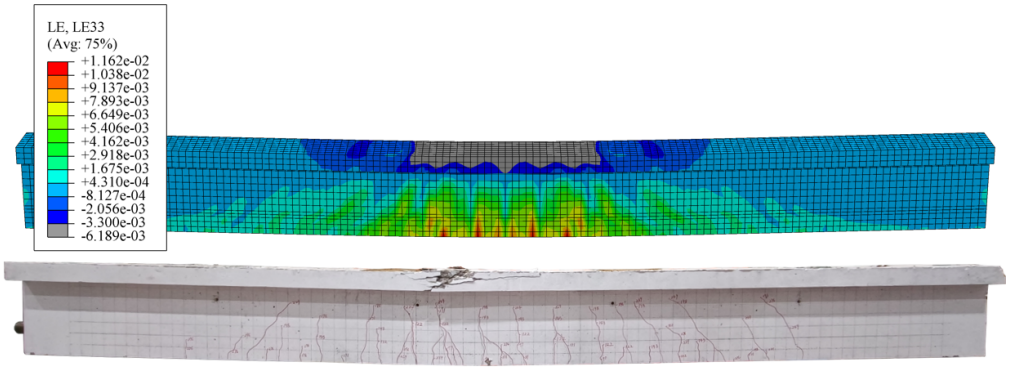


Figure 4. *Cont.*

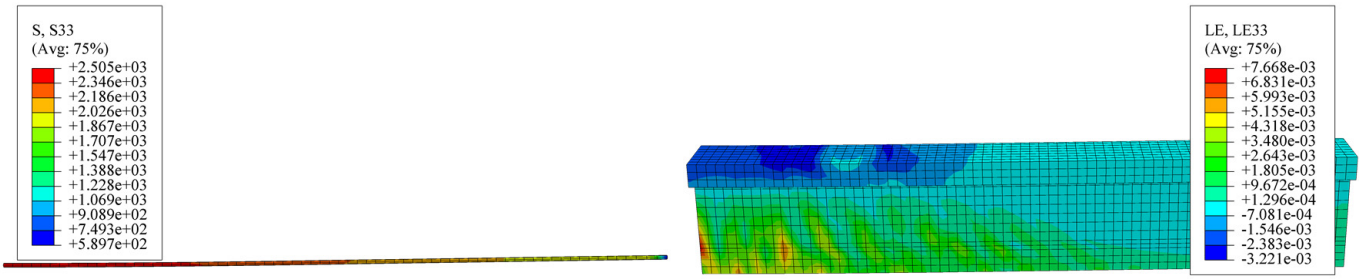


(**b**)

Figure 4. Comparison of the predicted and experimental failure modes of the typical specimens: (**a**) BS-30; (**b**) BS-60.

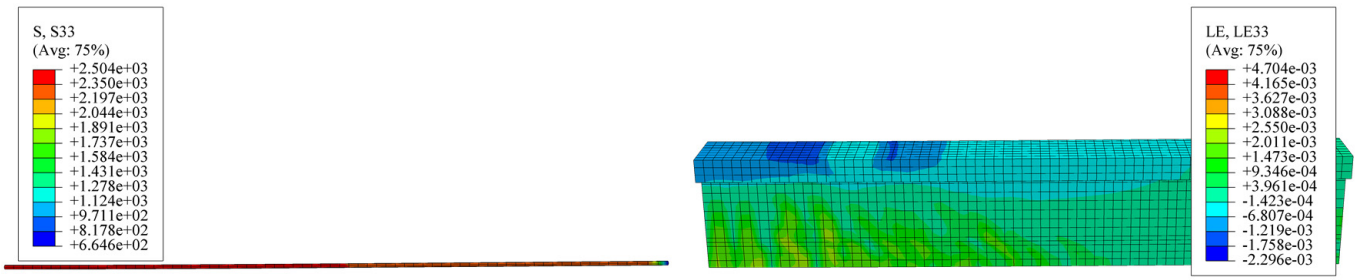
3.2.2. Effect of Prestress Level

In the previous experimental study [1], the prestress level varied from 30% to 60%, and the observed failure mode was concrete crushing. To further investigate the effect of prestress level, a wider range (from 0 to 90%) is explored in the numerical study. The numerical results indicated that as the prestress level increased, the failure mode shifted from concrete crushing to CFRP strand fracture. When the prestress level reached 80% and 90%, the CFRP strand fracture occurred before concrete crushing. As shown in Figures 5 and 6, the compressive strain in the concrete remained below the ultimate compressive strain of 0.0033, even when the tensile stress in the CFRP strands reached the ultimate strength of 2500 MPa.



(**a**) (**b**)

Figure 5. Tensile fracture failure of the CFRP strands in specimen BS-80: (**a**) tensile stress in the CFRP strand; (**b**) strain in the concrete.



(**a**) (**b**)

Figure 6. Tensile fracture failure of the CFRP strands in specimen BS-90: (**a**) tensile stress in the CFRP strand; (**b**) strain in the concrete.

The effect of prestress level on the flexural behavior is shown in Figure 7. It should be noted that for specimen BS-90, with a prestress level of 90%, the steel rebars did not yield at the moment the CFRP strands fractured. This was mainly due to the low usable stress (i.e., 250 MPa) that remained to bear the applied load, which is significantly lower than the yielding strength of the tensile rebars (467 MPa). As a result, the yielding load at a 90% prestress level is not included in Figure 7b. As the prestress level increased, both the cracking load and yielding load exhibited a generally linear trend. Specifically, the cracking load increased from 49.5 kN to 120.6 kN when the prestress level rose from 0 to 90%. Meanwhile, the yielding load increased from 237.3 kN to 316.3 kN as the prestress level increased from 0 to 80%. Compared to beam B-0 without CFRP strand reinforcement, the improvement in cracking and yielding loads ranged from 10.7% to 169.8% (for prestress levels from 0 to 90%) and 5.9% to 41.1% (for prestress levels from 0 to 80%), respectively. This indicates that the use of one non-prestressed CFRP strand did not significantly enhance the cracking and yielding loads. In contrast, the application of prestress was highly effective in increasing both the cracking and yielding loads. However, the ultimate load showed an initial increase followed by a drop as the prestress level increased from 0 to 90%. Specifically, the ultimate load increased from 291.3 kN to 324.6 kN as the prestress level increased from 0 to 80%, but then reduced to 273.9 kN at a prestress level of 90%. This reduction can be attributed to the premature fracture of the CFRP strands, which limited the effective use of the strength of both the steel rebars and the compressive concrete in this specimen. As mentioned earlier, when the CFRP strands reached their ultimate tensile strength, the tensile steel rebars did not yield, and the compressive concrete did not reach its ultimate state. In addition, Figure 7a shows that the ultimate deflection gradually decreased as the prestress level increased, with a particularly notable reduction observed under the CFRP strand fracture failure. From Table 4, it can be seen that the ultimate stress of the CFRP strands increased with the prestress level. However, it is crucial to note that under the CFRP strand fracture failure, the concrete strength (even the steel strength) was not fully utilized, and this type of failure often occurred suddenly due to the linear-elastic behavior of the CFRP strands. Therefore, in practical applications, CFRP strand fracture failure should be avoided, indicating that excessively high initial prestress in the CFRP strands should not be allowed.

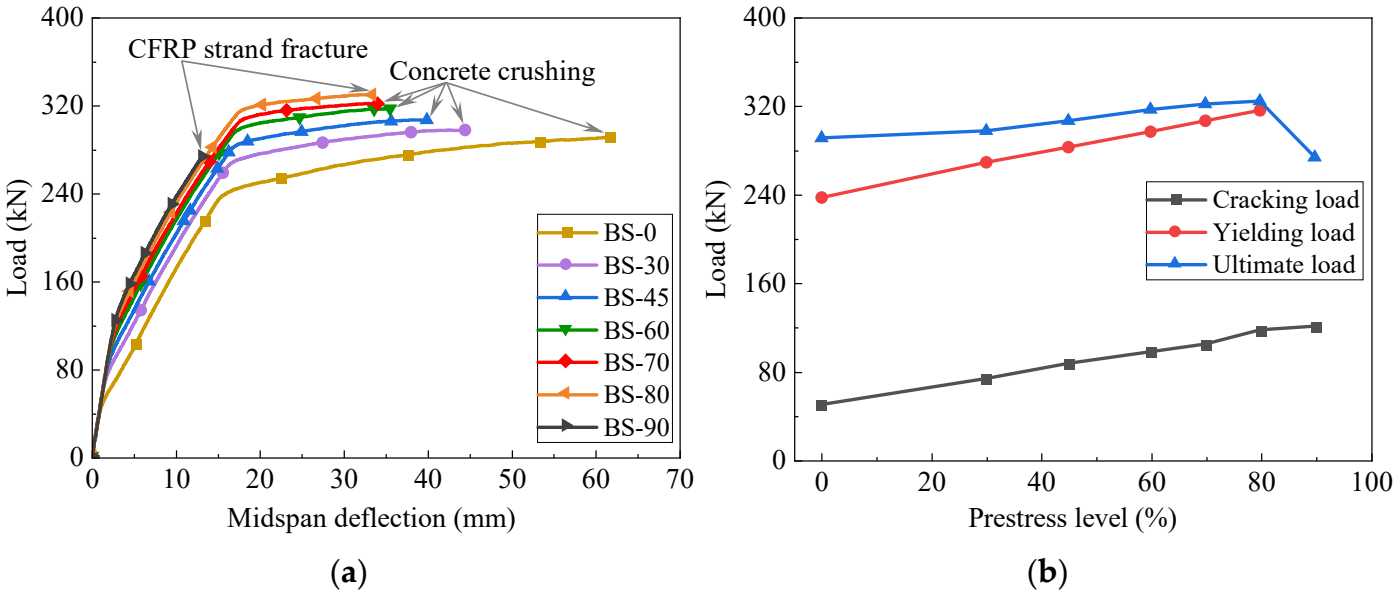


Figure 7. Effect of prestress level: (**a**) on the load-deflection curves; (**b**) on the characteristic loads.

3.2.3. Effect of Concrete Strength

To evaluate the effect of concrete strength on flexural behavior, PC beam models with three different concrete strength grades (C30, C40, and C50 in accordance with Chinese code [45]) were simulated. These specimens are designated as BS-60-C30, BS-60, and BS-60-C50, respectively, and their simulated results are shown in Figure 8. Clearly, under the same prestress level, increasing the concrete strength had a slight effect on the flexural stiffness of the PC beams. However, it enhanced the cracking load, yielding load, ultimate load, and ultimate deflection. Specifically, the cracking load increased from 92.2 kN to 110.0 kN, the yielding load rose from 293.7 kN to 301.1 kN, and the ultimate load increased from 308.5 kN to 340.2 kN. Notably, the increase in concrete strength had a more substantial improvement in the ultimate load compared to the cracking and yielding loads. Additionally, under the specimen conditions, the failure mode changed to CFRP strand fracture for C50 concrete, whereas compressive concrete crushing failure was observed for both C30 and C40 concrete. The above analysis indicates that increasing concrete strength is beneficial for increasing the utilization rate of the CFRP strands and improving flexural behavior. Therefore, prestressed CFRP strands are more suitable for use as prestressed reinforcements in PC beams made with higher-strength concrete. However, it is crucial to properly select the initial prestress level to eliminate the risk of CFRP strand fracture failure.

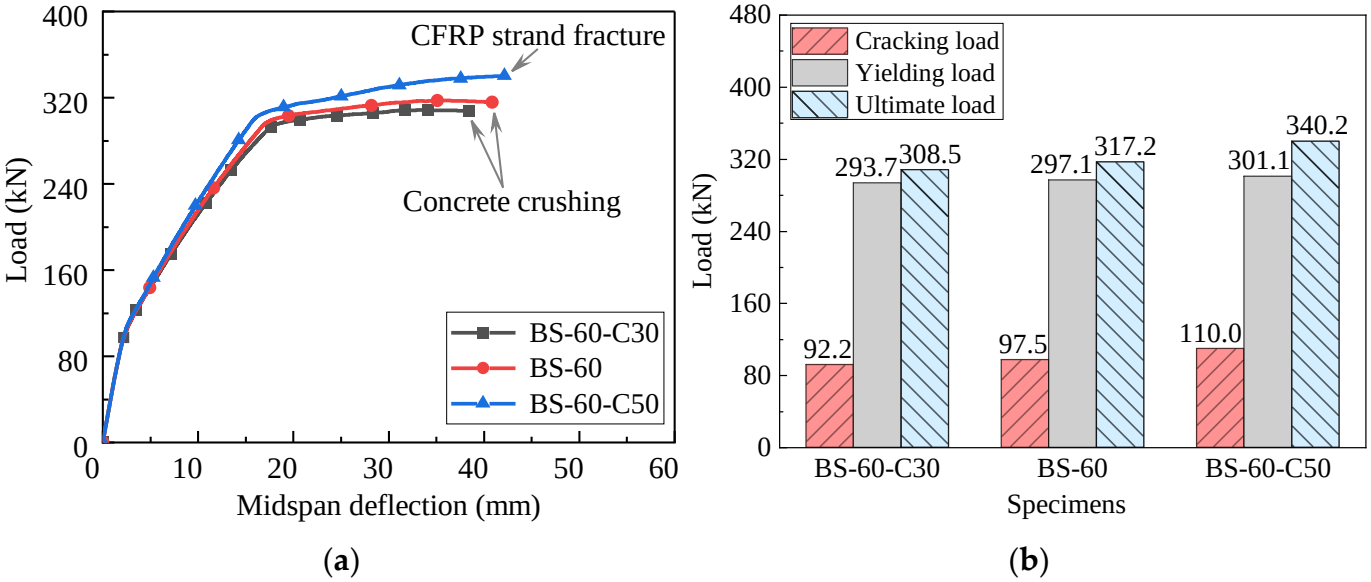


Figure 8. Effect of concrete strength: (**a**) on the load-deflection curves; (**b**) on the characteristic loads.

3.2.4. Effect of Steel Reinforcement Ratio

Three models (specimens BS-45, BS-45R, BS-45R#) with different steel reinforcement ratios were developed to evaluate the effect of the steel reinforcement ratio on the flexural behavior. Specimen BS-45 was reinforced with three tensile rebars of 22 mm diameter, BS-45R with two tensile rebars of 22 mm diameter, and BS-45R# with two tensile rebars of 20 mm diameter, which corresponded to the steel reinforcement ratios of 1.27%, 0.85%, and 0.70%, respectively. Figure 9 compares the load-deflection curves and the characteristic loads of the three specimens. As the steel reinforcement ratio increased, the cracking resistance exhibited minimal improvement, with only a 4.2 kN increase. However, both the yielding load and ultimate load increased significantly. The yielding load increased from 190.3 kN to 282.9 kN, an increase of 48.7%, while the ultimate load increased from 246.5 kN to 307.0 kN, a rise of 24.5%. Notably, when the steel reinforcement ratio decreased to 0.70%, the failure mode shifted from concrete crushing to CFRP strand fracture. Furthermore, as the steel reinforcement ratio decreased from 1.27% to 0.70%, the ultimate deflection of the PC beams and ultimate stress of the CFRP strands gradually increased, from 40.0 mm to

56.7 mm and from 1997 MPa to 2500 MPa, respectively. This indicates better ductility of the PC beams and a higher strength utilization ratio of the CFRP strands.

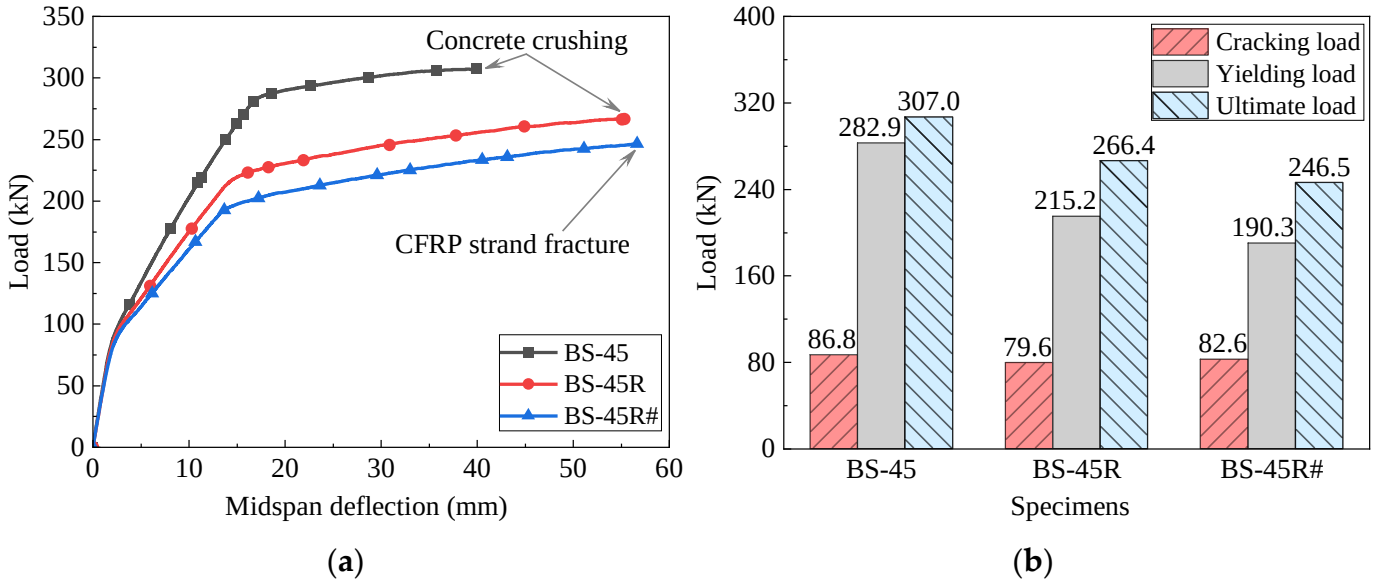


Figure 9. Effect of steel reinforcement ratio: (**a**) on the load-deflection curves; (**b**) on the characteristic loads.

4. ANN-Based Capacity Prediction

Artificial Neural Network (ANN) is an algorithmic model that mimics the behavior of animal neural networks and performs distributed and parallel information processing. Back Propagation ANN (BP-ANN) is one of the most widely used neural network models [39,40], characterized as a multi-layer feedforward network trained using an error backpropagation algorithm. The general architecture of the BP-ANN model is illustrated in Figure 10, which comprises an input layer, a hidden layer, and an output layer. The BP-ANN establishes a functional relationship from m independent variables to n dependent variables by utilizing connection weights (i.e., w_{ij} and w_{jk}) between the input layer and the hidden layer, and between the hidden layer and the output layer, as well as biases (i.e., a_j and b_k). During the training, the weights and biases at each neuron are iteratively adjusted to optimize the output and generate accurate predictions.

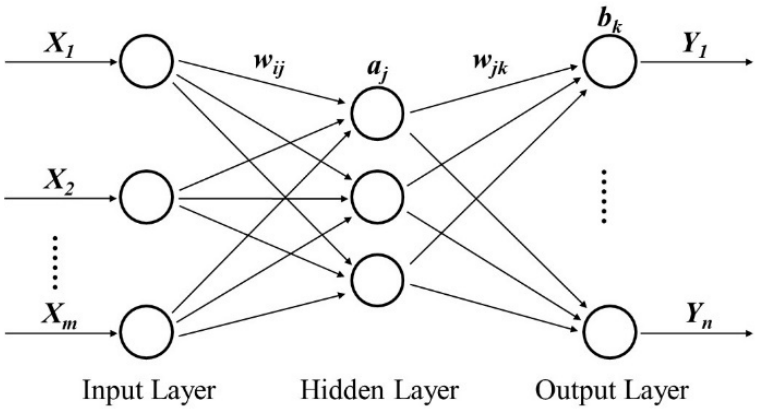


Figure 10. General architecture of BP-ANN model.

Due to the limited experimental data on PC beams reinforced with prestressed CFRP strands and non-prestressed steel rebars, the verified FE models were employed to generate the training database for the BP-ANN model. For PC T-beams reinforced with prestressed CFRP strands and non-prestressed steel bars, the ultimate flexural capacity is related to

the concrete strength, T-beam section size, cross-sectional area, and yielding strength of non-prestressed steel rebars, prestress level, ultimate strength and placement position of prestressed CFRP strands. To simplify the input variables, the sectional height of the T-beam and the placement height of non-prestressed tensile steel rebars were consolidated into one variable, represented by the effective depth of the T-beam, while the effect of the placement position of compressive steel rebars was disregarded. Finally, the input layer consisted of 14 variables: cross-sectional area A_1 (mm^2) and yielding strength f_1 (MPa) of non-prestressed tensile steel bars, cross-sectional area A_2 (mm^2) and yielding strength f_2 (MPa) of non-prestressed compressive steel rebars, concrete strength f_c (MPa), flange depth h_f (mm), flange width b_f (mm), web width b_w (mm), effective depth h_{eff} (mm), cross-sectional area A_{cf} (mm^2) and arrangement height h_{cf} (mm) of the CFRP strands, ultimate strength f_u (MPa), elastic modulus E_{cf} (MPa), and initial prestress f_p (MPa) of the CFRP strands. The ultimate moment M_u (kN·m) served as the output variable. The training database generated from the FE modeling is summarized in Table A1 in Appendix A.

The neural network toolbox in MATLAB [48] was used for conducting the ANN simulations. According to existing studies [39,40], a single hidden layer BP-ANN model was implemented. The number of nodes in the hidden layer, which significantly affects prediction accuracy, was determined to be 14 following the empirical approach [49,50]. The Levenberg–Marquardt (trainlm) algorithm was employed for training the BP-ANN, which has been successfully adopted and validated in other studies involving FRP-reinforced members [39]. This algorithm is a blend of gradient descent and the Gauss–Newton method, resulting in faster convergence with fewer iterations compared to alternative methods. MATLAB's default settings for the node transfer function, training function, and network learning function were utilized in the BP-ANN model. The maximum number of training epochs was set to 2000, the error goal was set at 1×10^{-6}, and the learning rate was 0.01. Figures 11 and 12 show the regression results for the training and test datasets. The correlation coefficients R for both the training and test datasets were approximately 0.99, demonstrating that the BP-ANN training achieved accurate results. Additionally, it can be found that the BP-ANN model did not exhibit an overfitting problem since the correlation coefficients for the test dataset closely matched those for the training dataset.

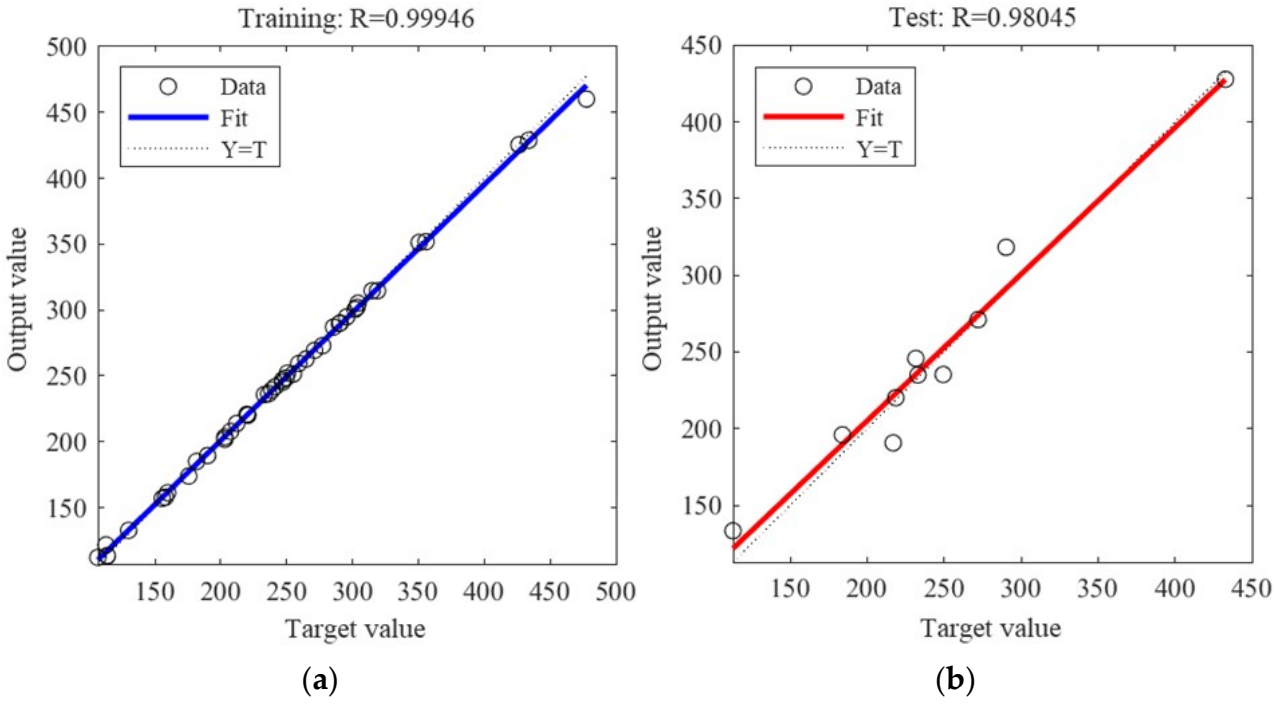


Figure 11. Regression of the PB-ANN model for concrete crushing mode: (**a**) training dataset; (**b**) test dataset.

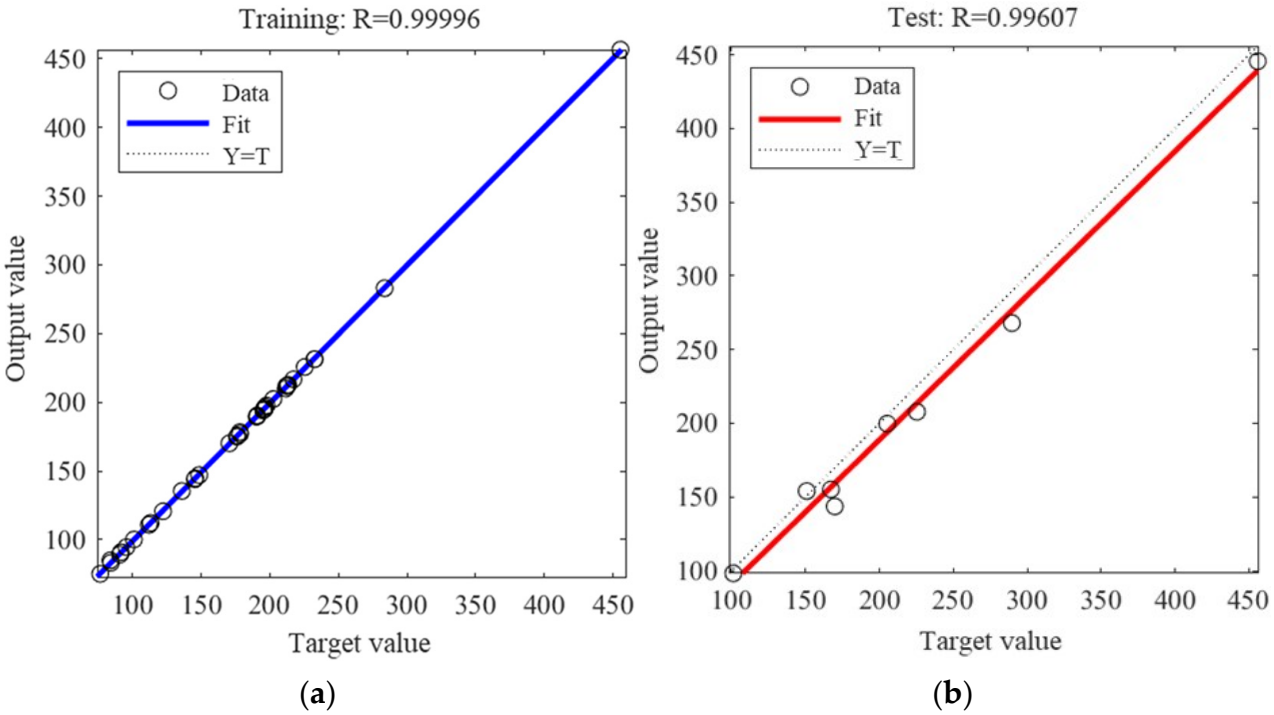


Figure 12. Regression of the PB-ANN model for CFRP strand fracture mode: (**a**) training dataset; (**b**) test dataset.

Furthermore, the ultimate flexural capacity of PC T-beams reinforced with bonded prestressed CFRP strands was predicted using the trained BP-ANN model. The predicted results and experimental results are compared in Table 5. It is noted that since the database used for training the BP-ANN model only included PC T-beams with straight bonded CFRP strands, only the experimental specimens BS-30, BS-45, BS-60, BD-30, and BS-45R are included in Table 5. Upon comparison, it was observed that despite the limited datasets used for training, the predicted results of the ultimate moment aligned well with the experimental results, with a maximum relative error of approximately 8%. This demonstrates the effectiveness of the BP-ANN model in predicting the ultimate flexural capacity of PC T-beams reinforced with bonded prestressed CFRP strands and non-prestressed steel rebars.

Table 5. Comparison of predicted and experimental ultimate moments from reference [1].

Specimen	Experimental Value (kN·m)	Predicted Value (kN·m)	Error (%)
BS-30	222.0	234.1	5.5
BS-45	238.5	241.8	1.4
BS-60	252.8	249.5	1.3
BD-30	261.0	272.9	4.6
BS-45R	195.8	211.7	8.1

However, it should be noted that as a preliminary investigation, only a limited amount of data from the FE modeling was included in the current database, with a relatively narrow range of input parameters. For instance, the sectional dimensions of the specimens listed in Table A1 were limited to small- and medium-scale, and high-strength concrete was not considered. Moreover, some factors such as the variability in the mechanical properties of materials and the assumptions made in the FE models also contributed to the prediction errors. Therefore, although the trained BP-ANN model accurately predicted the ultimate capacity of the experimental specimens, further validation is required to confirm

its generalizability to large-scale PC beams in real-world applications, which would benefit from additional training data and experimental tests.

5. Conclusions

This paper presents an investigation into the flexural capacity prediction of PC T-beams reinforced with prestressed CFRP strands and non-prestressed steel rebars using both FE modeling and BP-ANN methods. The main findings are summarized as follows:

(1) The developed three-dimensional FE models accurately predicted the flexural behavior of the PC T-beams, with relative errors between the numerical and experimental ultimate loads below 6%. The developed FE models provided a solid foundation for parametric studies and the creation of a database for training the BP-ANN;

(2) Compared to beams with non-prestressed CFRP strands, applying prestress significantly enhanced the flexural behavior. The ultimate load increased from 291.3 kN to 324.6 kN as the prestress level increased from 0% to 80%. However, at a prestress level of 90%, the ultimate load decreased to 273.9 kN due to the premature fracture of the CFRP strands and no yielding of the non-prestressed steel rebars. Therefore, excessively high initial prestress in the CFRP strands should not be allowed in practical applications;

(3) With an increase in the concrete strength, the ultimate load improvement was more significant than the improvements in cracking and yielding loads. Additionally, increasing the steel reinforcement ratio led to significant improvements in both ultimate and yielding loads, while having only a minor impact on the cracking load;

(4) The BP-ANN model demonstrated strong prediction capability for the ultimate capacity of experimental PC T-beams reinforced with prestressed CFRP strands and non-prestressed steel rebars. This suggests its potential as a rapid and reliable method for predicting the ultimate capacity of this type of PC beam in practical applications. However, future research should focus on gathering a more extensive dataset to further train the model and validate its generalizability to large-scale PC beams in real-world scenarios.

Author Contributions: Conceptualization, J.B., Y.Y. and G.-W.X.; investigation, H.-T.W., X.-J.L. and M.-S.C.; writing—original draft preparation, H.-T.W., X.-J.L. and M.-S.C.; writing—review and editing, H.-T.W. and X.-J.L.; project administration, J.B., Y.Y. and G.-W.X.; funding acquisition, H.-T.W., J.B., Y.Y. and G.-W.X. All authors have read and agreed to the published version of the manuscript.

Funding: This research was funded by the National Natural Science Foundation of China (52378233), the CSCEC Technology R&D Program (CSCEC-2022-Z-8), and the China Scholarship Council (202306710015).

Data Availability Statement: The data presented in this study are available in the article.

Conflicts of Interest: Authors Jie Bai, Yan Yang and Guo-Wen Xu were employed by the company China Construction Eighth Engineering Division Co., Ltd. The remaining authors declare that the research was conducted in the absence of any commercial or financial relationships that could be construed as a potential conflict of interest.

Appendix A

Table A1. Training database of the BP-ANN model.

A_1	f_1	A_2	f_2	f_c	h_{eff}	b_w	b_f	h_f	A_{cf}	f_u	h_{cf}	f_p	E_{cf}	M_u
982	420	200	500	20.1	270	150	300	50	120	2500	240	0	147,000	112.9
628	440	150	540	26.8	270	150	300	50	140	2500	220	750	160,000	112.8
1100	460	250	580	30.2	270	150	300	50	160	2500	200	1125	180,000	159.7
1300	480	200	620	33.5	270	150	300	50	120	2500	240	1500	147,000	190.0
982	400	150	500	20.1	270	150	300	50	140	2500	220	0	160,000	106.7

Table A1. *Cont.*

A_1	f_1	A_2	f_2	f_c	h_{eff}	b_w	b_f	h_f	A_{cf}	f_u	h_{cf}	f_p	E_{cf}	M_u
628	420	250	540	26.8	270	150	300	50	160	2500	200	750	180,000	113.8
1100	440	200	580	30.2	270	150	300	50	120	2500	240	1125	147,000	157.9
1300	460	150	620	33.5	270	150	300	50	140	2500	220	1500	160,000	181.6
982	480	250	540	20.1	270	150	300	50	160	2500	200	750	180,000	130.1
628	400	200	580	26.8	270	150	300	50	120	2500	220	1125	160,000	113.9
1100	440	150	620	30.2	270	150	300	50	140	2500	200	1500	180,000	153.4
1000	420	200	500	20.1	370	150	350	75	220	2500	340	0	147,000	207.4
1000	440	150	540	26.8	370	150	350	75	140	2500	320	750	160,000	233.0
1200	460	250	580	30.2	370	150	350	75	160	2500	300	1125	180,000	282.7
1200	480	200	620	30.2	370	150	350	75	180	2500	340	1500	147,000	314.9
1300	400	150	500	20.1	370	150	350	75	200	2500	320	0	160,000	212.1
1300	420	250	540	26.8	370	150	350	75	220	2500	300	750	180,000	272.1
1400	440	200	580	30.2	370	150	350	75	160	2500	340	1125	147,000	304.2
1000	460	150	620	20.1	370	150	350	75	160	2500	320	1500	160,000	231.6
1200	480	250	540	26.8	370	150	350	75	180	2500	300	0	180,000	255.1
1200	400	200	580	30.2	370	150	350	75	200	2500	340	750	160,000	285.6
1300	440	150	620	33.5	370	150	350	75	220	2500	320	1125	180,000	319.0
1300	420	200	500	20.1	370	150	350	75	140	2500	300	1500	147,000	236.4
1000	440	150	540	26.8	370	150	350	75	160	2500	340	750	160,000	247.0
1000	460	200	560	30.2	370	150	350	75	180	2500	320	1125	180,000	277.3
1200	420	160	500	20.1	370	150	350	75	180	2500	300	1200	160,000	228.4
1500	420	200	500	26.8	470	200	400	100	170	2500	440	750	160,000	433.8
1000	440	150	540	20.1	470	200	400	100	200	2500	420	1125	180,000	355.8
1200	460	250	580	20.1	470	200	400	100	300	2500	400	1500	147,000	426.4
1400	480	200	620	30.2	470	200	400	100	250	2500	440	0	160,000	477.6
1200	400	150	500	20.1	470	200	400	100	200	2500	420	750	180,000	350.6
1000	420	250	540	26.8	470	200	400	100	300	2500	400	1125	160,000	432.8
1400	440	150	550	20.1	470	200	400	100	250	2500	440	1500	180,000	442.2
1200	420	200	500	20.1	320	200	400	75	220	2500	290	0	147,000	193.1
1400	440	150	540	26.8	320	200	400	75	140	2500	250	750	160,000	224.6
1200	460	250	580	30.2	320	200	400	75	160	2500	270	750	180,000	247.0
1400	480	200	620	33.5	320	200	400	75	180	2500	290	1500	147,000	302.0
900	400	150	500	20.1	320	200	400	75	200	2500	250	0	160,000	155.6
1200	420	250	540	26.8	320	200	400	75	220	2500	270	750	180,000	238.8
1400	440	200	580	30.2	320	200	400	75	140	2500	290	1125	147,000	259.2
1200	460	150	620	30.2	320	200	400	75	160	2500	250	1500	160,000	241.3
800	480	250	540	20.1	320	200	400	75	180	2500	270	0	180,000	175.7
900	400	200	580	26.8	320	200	400	75	200	2500	290	750	160,000	219.9
1200	440	150	620	30.2	320	200	400	75	220	2500	250	1125	180,000	246.2
1400	420	200	500	20.1	320	200	400	75	140	2500	270	1500	147,000	218.6
1000	440	150	540	26.8	320	200	400	75	160	2500	290	0	160,000	203.1
1500	460	250	580	30.2	320	200	400	75	180	2500	250	750	180,000	264.7
1200	480	200	620	33.5	320	200	400	75	200	2500	270	1125	147,000	271.2
1200	400	150	500	20.1	320	200	400	75	220	2500	290	1500	160,000	224.7
1400	420	250	540	26.8	320	200	400	75	140	2500	250	0	180,000	216.9
1000	440	200	580	30.2	320	200	400	75	160	2500	270	750	147,000	220.6
1000	460	150	620	33.5	320	200	400	75	220	2500	260	1125	160,000	249.4
900	480	250	540	20.1	320	200	400	75	200	2500	250	1500	180,000	203.1
1200	440	150	620	30.2	320	200	400	75	250	2500	270	1125	160,000	262.1
1000	420	200	500	20.1	320	200	500	75	150	2500	290	750	147,000	206.9
1200	440	150	540	26.8	320	200	500	75	200	2500	250	1125	160,000	249.5
1400	460	250	580	30.2	320	200	500	75	250	2500	220	1500	180,000	290.3
800	400	150	500	20.1	360	250	400	75	150	2500	300	750	147,000	183.9
1200	420	250	500	26.8	360	250	400	75	130	2500	300	1000	160,000	250.6
1400	440	200	580	20.1	360	250	400	75	170	2500	340	1500	180,000	290.7
1400	460	150	620	33.5	360	250	400	75	150	2500	300	750	147,000	295.6
1000	480	250	500	20.1	360	250	400	75	130	2500	320	1125	160,000	233.2
1200	460	200	160	26.8	360	250	400	75	170	2500	340	1500	180,000	303.4

Table A1. *Cont.*

A_1	f_1	A_2	f_2	f_c	h_{eff}	b_w	b_f	h_f	A_{cf}	f_u	h_{cf}	f_p	E_{cf}	M_u
1400	440	150	580	30.2	360	250	400	75	150	2500	300	1125	160,000	290.0
628	400	314	400	26.8	270	150	300	50	80	2500	240	871	147,000	101.1
402	400	314	400	26.8	270	150	300	50	80	2500	240	870	147,000	84.3
402	400	201	400	26.8	270	150	300	50	139	2500	240	1225	147,000	112.0
226	400	201	400	26.8	270	150	300	50	139	2500	240	1225	147,000	98.2
628	400	452	400	26.8	270	150	300	50	139	2500	240	1225	147,000	134.8
628	400	616	400	26.8	270	150	300	50	139	2500	240	1225	147,000	136.0
628	400	201	400	26.8	270	150	300	50	99	2500	240	1225	147,000	113.2
628	400	201	400	26.8	270	150	300	50	59	2500	240	1225	147,000	95.5
628	400	201	400	26.8	370	150	350	75	139	2500	340	1250	147,000	190.8
628	400	201	400	30.2	370	150	350	75	139	2500	340	1581	147,000	196.5
1200	400	201	400	30.2	370	150	350	75	180	2500	340	1625	147,000	289.7
1200	400	201	400	26.8	470	200	400	100	260	2500	440	1250	147,000	456.0
1200	400	201	400	30.2	470	200	400	100	260	2500	440	1250	147,000	454.0
1200	400	201	400	33.5	470	200	400	100	260	2500	440	1250	147,000	455.4
1000	400	201	400	26.8	320	200	400	75	139	2500	260	1250	147,000	190.4
1000	400	320	400	26.8	320	200	400	75	139	2500	260	1250	147,000	195.2
1000	400	500	400	26.8	320	200	400	75	139	2500	260	1250	147,000	196.5
1000	400	201	350	26.8	320	200	400	75	139	2500	260	1250	147,000	196.0
1000	450	320	452	30.2	320	200	400	75	139	2500	260	1250	147,000	212.1
1000	432	500	353	33.5	320	200	400	75	139	2500	260	1250	147,000	213.0
1200	400	201	452	30.2	320	200	400	75	139	2500	240	1000	180,000	202.6
1000	432	500	353	33.5	320	200	400	75	230	2500	220	1500	180,000	247.2
600	400	201	400	26.8	320	200	400	75	139	2500	290	1250	147,000	161.4
500	400	201	400	26.8	320	200	400	75	139	2500	290	1250	147,000	150.8
800	400	201	400	26.8	320	200	400	75	139	2500	290	1250	147,000	176.6
800	600	320	600	26.8	320	200	400	75	139	2500	290	1250	147,000	217.2
1000	432	500	353	33.5	320	200	400	75	139	2500	290	1250	147,000	213.0
600	450	400	500	26.8	320	200	400	75	230	2500	290	736	147,000	213.4
400	400	201	400	26.8	320	200	500	75	139	2500	290	1250	147,000	145.4
600	400	300	400	26.8	320	200	500	75	139	2500	290	1250	147,000	167.2
1000	400	201	400	26.8	320	200	500	75	200	2500	290	1250	147,000	232.5
400	400	201	400	26.8	320	200	500	75	200	2500	290	1250	147,000	178.4
400	400	201	400	26.8	320	200	500	75	300	2500	290	1250	147,000	225.4
1000	400	201	400	26.8	320	200	500	75	200	2500	250	1665	200,000	232.8
628	400	314	400	20.1	270	150	300	50	80	1800	240	871	147,000	91.0
402	400	314	400	20.1	270	150	300	50	80	2000	240	870	160,000	73.5
402	400	201	400	23.5	270	150	300	50	139	2200	240	1225	175,000	101.2
226	400	201	400	23.5	270	150	300	50	139	2400	240	1225	190,000	91.6
628	400	201	400	26.8	270	150	300	50	59	1800	240	871	190,000	83.9
628	400	201	400	26.8	370	150	350	75	139	2000	340	870	147,000	169.8
628	400	201	400	30.2	370	150	350	75	139	2200	340	1225	160,000	178.2
1200	400	201	400	30.2	370	150	350	75	180	2400	340	1225	175,000	283.6
1000	400	201	400	26.8	320	200	400	75	139	1800	260	871	175,000	170.6
1200	400	201	400	26.8	320	200	400	75	139	2000	260	870	190,000	197.7
1400	400	320	400	26.8	320	200	400	75	139	2200	260	1225	147,000	225.5
1000	400	500	400	26.8	320	200	400	75	139	2400	260	1225	160,000	191.0
500	400	201	400	26.8	320	200	400	75	139	1800	290	871	160,000	122.3
800	400	201	400	26.8	320	200	400	75	139	2000	290	870	175,000	163.2
800	600	320	600	23.5	320	200	400	75	139	2200	290	1225	190,000	212.9
1000	432	500	353	23.5	320	200	400	75	139	2400	290	1225	147,000	207.7
400	400	201	400	26.8	320	200	500	75	139	2800	290	1600	175,000	145.7
600	400	300	400	26.8	320	200	500	75	139	3000	290	1600	190,000	176.1
1000	400	201	400	26.8	320	200	500	75	200	1800	290	1250	147,000	205.3
400	400	201	400	23.5	320	200	500	75	200	2000	290	1250	160,000	148.6
400	400	201	400	23.5	320	200	500	75	300	2200	290	1250	175,000	211.6
400	400	201	400	26.8	320	200	500	75	50	2600	290	1250	147,000	76.6

References

1. Wang, H.T.; Tang, C.; Chen, M.S.; Shi, J.Z.; Cao, X.Y. Experimental study on the flexural performance of prestressed RC beams with post-tensioned CFRP strands. *Eng. Struct.* **2024**, *309*, 118118. [CrossRef]
2. Campione, G.; Zizzo, M. Influence of strands corrosion on the flexural behavior of prestressed concrete beams. *Structures* **2022**, *45*, 1366–1375. [CrossRef]
3. Kioumarsi, M.; Benenato, A.; Ferracuti, B.; Imperatore, S. Residual flexural capacity of corroded prestressed reinforced concrete beams. *Metals* **2021**, *11*, 442. [CrossRef]
4. Carola Bridge Dresden: Possible Cause of the Collapse and History. Available online: https://www.diesachsen.de/en/various-news/carola-bridge-dresden-possible-cause-of-the-collapse-and-history-2954124 (accessed on 20 October 2024).
5. Yin, W.; Jiang, C.; Nagai, K. Mesoscale discrete simulation of flexural behavior of FRP-strengthened RC beams using 3D RBSM. *Eng. Struct.* **2024**, *310*, 118131. [CrossRef]
6. Wang, H.T.; Bian, Z.N.; Xu, G.W.; Chen, M.S.; Xiong, H.; Liu, S.S. Flexural strengthening of large-scale RC beams with non-prestressed and prestressed CFRP using different anchorages. *Polymers* **2022**, *14*, 5498. [CrossRef]
7. Li, C.G.; Xian, G.J. Novel wedge-shaped bond anchorage system for pultruded CFRP plates. *Mater. Struct.* **2018**, *51*, 162. [CrossRef]
8. Shi, J.W.; Wu, Q.Q.; Li, B.; Liu, Y.; Cao, W.H.; Wang, H.T. Fatigue bond behavior of FRP-to-concrete joints with various bonding adhesives. *Eng. Struct.* **2024**, *301*, 117311. [CrossRef]
9. Li, C.G.; Xian, G.J. Design optimization and experimental validation of a novel wedge-shaped bond anchorage system for prestressed CFRP plates. *Polym. Test.* **2019**, *75*, 167–174. [CrossRef]
10. Jiang, C.; Yu, Q.Q.; Gu, X.L. A unified bond-slip model for the interface between FRP and steel. *Compos. Part B-Eng.* **2021**, *277*, 109380. [CrossRef]
11. Pang, Y.Y.; Wu, G.; Wang, H.T.; Su, Z.L.; He, X.Y. Experimental study on the bond behavior of the CFRP-steel interface under the freeze–thaw cycles. *J. Compos. Mater.* **2020**, *54*, 13–29. [CrossRef]
12. Pang, Y.Y.; Wu, G.; Wang, H.T.; Gao, D.Y.; Zhang, P. Experimental study on the bond behavior of the CFRP-steel interface under rapid loading. *Thin-Walled Struct.* **2021**, *159*, 107233. [CrossRef]
13. Wang, H.T.; Wu, Q.; Li, L.; Wei, F.F.; Zhu, D.C.; Yu, X.P. Mechanical behaviors of steel-CFRP plate bonded joints after freezing-thawing cycles. *Constr. Build. Mater.* **2024**, *412*, 134876. [CrossRef]
14. Jiang, C. Strength enhancement due to FRP confinement for coarse aggregate-free concretes. *Eng. Struct.* **2023**, *277*, 115370. [CrossRef]
15. Xian, G.J.; Guo, R.; Li, C.G.; Wang, Y.J. Mechanical performance evolution and life prediction of prestressed CFRP plate exposed to hygrothermal and freeze-thaw environments. *Compos. Struct.* **2022**, *293*, 115719. [CrossRef]
16. Wang, X.; Shi, J.; Wu, G.; Yang, L.; Wu, Z. Effectiveness of basalt FRP tendons for strengthening of RC beams through the external prestressing technique. *Eng. Struct.* **2015**, *101*, 34–44. [CrossRef]
17. Xian, G.J.; Bai, Y.B.; Zhou, P.; Wang, J.Q.; Li, C.G.; Dong, S.C.; Guo, R.; Tian, J.W.; Li, J.H.; Zhong, J.; et al. Long-term properties evolution and life prediction of glass fiber reinforced thermoplastic bending bars exposed in concrete alkaline environment. *J. Build. Eng.* **2024**, *91*, 109641. [CrossRef]
18. Chen, L.; Qiang, X.; Sun, P.; Zhang, S.; Jiang, X. Experimental and Theoretical Study on Flexural Behavior of Prestressed Concrete Beams Strengthened by CFRP Tendons with External unbonded Retrofit System. *J. Build. Eng.* **2024**, *89*, 109301. [CrossRef]
19. Wang, H.T.; Liu, S.S.; Shi, J.W.; Xu, G.W.; Chen, M.S.; Bian, Z.N. Bonded and unbonded strengthening of RC beams with the prestressed CFRP plate system: An experimental study. *Constr. Build. Mater.* **2024**, *438*, 137118. [CrossRef]
20. Wang, H.T.; Wu, Q.; Zhu, C.Y.; Mao, Y.H.; Guo, C.C. An innovative prestressing system of prestressed carbon fiber sheets for strengthening RC beams under flexure. *Constr. Build. Mater.* **2024**, *411*, 134409. [CrossRef]
21. Wang, H.T.; Bian, Z.N.; Wu, Q.; Hu, L.; Chen, M.S.; Tang, C. Development of a novel anchorage and tensioning system for strengthening steel beams with unbonded prestressed CFRP plates. *Eng. Struct.* **2024**, *312*, 118234. [CrossRef]
22. Wang, H.T.; Bian, Z.N.; Chen, M.S.; Hu, L.; Wu, Q. Flexural strengthening of damaged steel beams with prestressed CFRP plates using a novel prestressing system. *Eng. Struct.* **2023**, *284*, 115953. [CrossRef]
23. Wang, H.T.; Liu, S.S.; Zhu, C.Y.; Xiong, H.; Xu, G.W. Experimental study on the flexural behavior of large-scale reinforced concrete beams strengthened with prestressed CFRP plates. *J. Compos. Constr.* **2022**, *26*, 04022076. [CrossRef]
24. Atutis, M.; Valivonis, J.; Atutis, E. Analysis of serviceability limit state of GFRP prestressed concrete beams. *Compos. Struct.* **2015**, *134*, 450–459. [CrossRef]
25. Saafi, M.; Toutanji, H. Flexural capacity of prestressed concrete beams reinforced with aramid fiber reinforced polymer (AFRP) rectangular tendons. *Constr. Build. Mater.* **1998**, *12*, 245–249. [CrossRef]
26. Heo, S.; Shin, S.; Lee, C. Flexural behavior of concrete beams internally prestressed with unbonded carbon-fiber-reinforced polymer tendons. *J. Compos. Constr.* **2013**, *17*, 167–175. [CrossRef]
27. Peng, F.; Xue, W.C. Design approach for flexural capacity of concrete T-beams with bonded prestressed and non-prestressed FRP reinforcements. *Compos. Struct.* **2018**, *204*, 333–341. [CrossRef]
28. Peng, F.; Xue, W.C. Analytical Approach for Flexural Capacity of FRP Prestressed Concrete T-Beams with Non-Prestressed Steel Bars. *J. Compos. Constr.* **2018**, *22*, 04018063. [CrossRef]

29. Wang, H.T.; Lin, J.Y.; Chen, L.; Shi, J.Z.; He, Y.H. Experimental study and model evaluation on BFRP tube-confined RAC cylinders under monotonic axial compression. *Structures* **2024**, *69*, 107307. [CrossRef]
30. Kim, Y.J. Flexural Response of Concrete Beams Prestressed with AFRP Tendons: Numerical Investigation. *J. Compos. Constr.* **2010**, *14*, 647–658. [CrossRef]
31. Lou, T.; Liu, M.; Lopes, S.M.R.; Lopes, A.V. Effect of bond on flexure of concrete beams prestressed with FRP tendons. *Compos. Struct.* **2017**, *173*, 168–176. [CrossRef]
32. Motwani, P.; Rather, A.I.; Laskar, A. Transfer stage parameters for concrete beams prestressed with BFRP bars: Experimental and finite element studies. *Constr. Build. Mater.* **2022**, *315*, 125639. [CrossRef]
33. Bedon, C.; Louter, C. Numerical analysis of glass-FRP post-tensioned beams—-Review and assessment. *Compos. Struct.* **2017**, *177*, 129–140. [CrossRef]
34. Peng, F.; Xue, W.C.; Yu, T.Q. Cyclic behavior of polypropylene fiber reinforced concrete beams with prestressed CFRP tendons and non-prestressed steel bars. *Eng. Struct.* **2023**, *275*, 115201. [CrossRef]
35. Khalafalla, O.; Pour-Ghaz, M.; ElSafty, A.; Rizkalla, S. Durability of CFRP strands used for prestressing of concrete structural members. *Constr. Build. Mater.* **2019**, *228*, 116756. [CrossRef]
36. Li, Z.; Jiang, Z.; Fang, Z.; Wang, Z.; Fang, Y. High-temperature axial tensile property and fire resisting performance of CFRP strand cable. *Constr. Build. Mater.* **2024**, *421*, 135746. [CrossRef]
37. Wang, C.; Guan, S.; Sabbrojjaman, M.; Tafsirojjaman, T. Bond performance of CFRP strands to grouting admixture for prestressed structure and development of their bond–slip constitutive models. *Polymers* **2023**, *15*, 2906. [CrossRef]
38. Dahou, Z.; Sbartaï, Z.M.; Castel, A.; Ghomari, F. Artificial neural network model for steel–concrete bond prediction. *Eng. Struct.* **2009**, *31*, 1724–1733. [CrossRef]
39. Hu, L.L.; Feng, P.; Meng, Y.R.; Yang, J. Buckling behavior analysis of prestressed CFRP-reinforced steel columns via FEM and ANN. *Eng. Struct.* **2021**, *245*, 112853. [CrossRef]
40. Zarringol, M.; Patel, V.I.; Liang, Q.Q. Artificial neural network model for strength predictions of CFST columns strengthened with CFRP. *Eng. Struct.* **2023**, *281*, 115784. [CrossRef]
41. Khodadadi, N.; Roghani, H.; Caso, F.D.; El-kenawy, E.S.M.; Yesha, Y.; Nanni, A. Data-driven PSO-CatBoost machine learning model to predict the compressive strength of CFRP-confined circular concrete specimens. *Thin-Walled Struct.* **2024**, *198*, 111763. [CrossRef]
42. Ke, Y.; Zhang, S.S.; Jedrzejko, M.J.; Lin, G.; Li, W.G.; Nie, X.F. Strength models of near-surface mounted (NSM) fibre-reinforced polymer (FRP) shear-strengthened RC beams based on machine learning approaches. *Compos. Struct.* **2024**, *337*, 118045. [CrossRef]
43. Mohammadi, A.; Barros, J.A.O.; Sena-Cruz, J. An interpretable machine learning-based model for shear resistance prediction of CFRP-strengthened RC beams using experimental and synthetic dataset. *Compos. Struct.* **2025**, *351*, 118632. [CrossRef]
44. Zhang, T.; Gao, D.; Xue, C. Flexural strength prediction of concrete beams reinforced with hybrid FRP and steel bars based on machine learning. *Structures* **2024**, *65*, 106652. [CrossRef]
45. *GB 50010-2010*; Code for Design of Concrete Structures. China Architecture & Building Press: Beijing, China, 2015.
46. Mahmoud, M.R.I.; Wang, X.; Altayeb, M.; Al-Shami, H.A.M.; Ali, Y.M.S.; Moussa, A.M.A. Experimental and numerical study of the flexural behaviour of semi-precast slab reinforced with prestressed FRP bars. *Structures* **2024**, *62*, 106197. [CrossRef]
47. Wang, C.Y. *Simulation of Interfacial Bond Property FRP Reinforced Concrete Based on CZM*; Dalian University of Technology: Dalian, China, 2017.
48. MathWorks. *Neural Networks Toolbox Release R2019b*; Matlab: Natick, MA, USA, 2019.
49. Shen, H.Y.; Wang, Z.X.; Gao, C.Y.; Qin, J.; Yao, F.B.; Xu, W. Determining the number of BP neural network hidden layer units. *J. Tianjin Univ. Technol.* **2008**, *24*, 13–15.
50. Sheela, K.G.; Deepa, S.N. Review on Methods to Fix Number of Hidden Neurons in Neural Networks. *Math. Probl. Eng.* **2013**, *2013*, 425740. [CrossRef]

Disclaimer/Publisher's Note: The statements, opinions and data contained in all publications are solely those of the individual author(s) and contributor(s) and not of MDPI and/or the editor(s). MDPI and/or the editor(s) disclaim responsibility for any injury to people or property resulting from any ideas, methods, instructions or products referred to in the content.